

---

This is the **accepted version** of the journal article:

Fraxedas, Jordi; Schütte, Max; Sauthier, Guillaume; [et al.]. «In situ XPS analysis of the electronic structure of silicon and titanium thin films exposed to low-pressure inductively-coupled RF plasma». Applied surface science, Vol. 542 (March 2021), art. 148684. DOI 10.1016/j.apsusc.2020.148684

---

This version is available at <https://ddd.uab.cat/record/287270>

under the terms of the  license

# **In situ XPS analysis of the electronic structure of silicon and titanium thin films exposed to low-pressure inductively-coupled RF plasma**

Jordi Fraxedas <sup>a,b,\*</sup>, Max Schütte <sup>b</sup>, Guillaume Sauthier <sup>a</sup>, Massimo Tallarida <sup>b</sup>, Salvador Ferrer <sup>b</sup>, Vincent Carlino <sup>c</sup> and Eric Pellegrin <sup>d</sup>

<sup>a</sup>Catalan Institute of Nanoscience and Nanotechnology (ICN2), CSIC and BIST, Campus UAB, Bellaterra, Barcelona, 08193, Spain

<sup>b</sup>CELLS-ALBA, Carrer de la Llum 2-26, Cerdanyola del Valles, Barcelona, 08290, Spain

<sup>c</sup> IBSS Group Inc., Burlingame, CA 94010, USA.

<sup>d</sup> Carl Zeiss SMT GmbH, 73447 Oberkochen, Germany

\* Electronic mail: jordi.fraxedas@icn2.cat

## **Abstract**

Carbon contamination of synchrotron and free-electron lasers beamline optics continues to be a major nuisance due to the interaction of the intense photon beams with the surfaces of the optical elements in the presence of residual gases even in ultrahigh vacuum (UHV) conditions. Among the available in situ cleaning strategies, low-pressure radio frequency (RF) plasma treatment has emerged as a useful and relatively simple approach to remove such carbon contamination. However, the irreversible damage that the plasma may induce in such critical surfaces has to be carefully characterized before its general application. In this study, we focus on reducing the amount of carbon from UHV chamber inside surfaces via silicon and titanium coatings using a low-pressure inductively-coupled downstream plasma source and we characterize the surface alterations by in situ X-ray photoemission spectroscopy (XPS). The in situ mirror cleaning is simulated by means of silicon wafers. We observe upward band bending, which translates into lower binding energies of the photoemission lines, that we attribute to the generation of vacancies and trapped charges in the oxide layers.

**Keywords:** carbon contamination, thin-film coatings, ultrahigh vacuum chamber walls, inductively-coupled RF plasma, titanium oxide, silicon oxide, surface defects, band bending, X-ray photoemission spectroscopy.

## 1. Introduction

Carbon contamination of beamline optics in synchrotron radiation (SR) and free-electron laser (FEL) facilities has been over the years a major problem since it degrades the transmitted beams from mirrors and monochromators. Upon exposure to the photon beam in UHV conditions, a carbon layer builds up on the optical surface [1] inducing a detrimental reduction in reflectivity in particular in the vacuum ultraviolet (VUV) and soft X-ray regions with a loss of flux above the C K-edge and even at photon energies around 1 keV [2], which hinders the proper use of, e.g., absorption spectroscopies in that energy range.

Several methods have been proposed for the removal of carbon contamination mainly using oxygen, with a strong preference for those performed in situ over the time-consuming and rather elaborate ex situ cleaning techniques. In situ cleaning with oxygen activated by zeroth-order (white) SR light is perhaps the simplest and easiest method to implement, which consists in exposing the contaminated areas to an oxygen atmosphere (about  $10^{-4}$ - $10^{-6}$  mbar) while simultaneously irradiating with photons [3,4]. In situ use of reactive glow discharge [5] and of ozone generated via ultraviolet (UV) lamps [6] has also been reported with proven efficiency. In addition, in situ cleaning using different plasma discharge sources in different configurations adapted to the particular optical systems with pure oxygen or mixtures with other gases (hydrogen, water, argon, nitrogen, etc.) has also shown to be effective in removing carbon contamination [7–12].

However, one of the problems associated with plasma cleaning is the damage that the generated reactive species (ions, radicals, electrons, etc.) can induce in the exposed surfaces which can lead to modifications in their chemical composition, to an increase of the surface roughness and to contamination from the sputtering of the surrounding vacuum walls. In addition, the plasma may affect materials located in the vicinity of the optical elements such as cables, gauges, motors, etc., so that their location in the chamber has to be judiciously engineered, as well as the pumping distribution [13].

Here, we have explored the changes induced by oxygen and argon plasmas in the surface electronic structure of two selected UHV chamber wall coatings using in situ XPS, to avoid exposure of such surfaces to the atmosphere after plasma cleaning and thus visualize the direct effect on such surfaces [14–17]. The use of such coatings

pursuits the drop of both the outgassing and degassing from the UHV chamber inner walls with materials whose surfaces can become carbon-free upon exposure to an oxygen plasma, thus reducing the segregation and emission of carbon species into the vacuum volume of the UHV chamber. We have selected an inductively-coupled plasma (ICP) source with a downstream configuration to facilitate the strategic installation of adequate sources in vacuum vessels [10,11]. We have also studied the effect of the plasma on silicon wafers since silicon is commonly used in X-ray optics [18,19] and to be compared to the silicon vacuum chamber wall coatings mentioned above. The effect of oxygen plasma on the electronic structure of silicon has been largely discussed since it is a relevant growth technique of thin oxide layers and the control of the density and nature of defects is of enormous importance for the micro/nano-electronics industry [20,21].

## 2. Experimental details

The in situ cleaning of Si- and Ti-coated 304L stainless steel (SS304L) foils and of Si wafers using a low-pressure inductively-coupled GV10x DS (downstream) Asher plasma source<sup>1</sup> has been characterized by means of XPS. CVD-grown a:Si-H coatings (Silcolloy® 1000, thickness  $\approx 500$  nm) were provided by SilcoTek, PA, USA and  $\approx 200$  nm thick Ti films were deposited ex situ by e-beam evaporation at the Catalan Institute of Nanoscience and Nanotechnology (ICN2). The SS304L substrates (0.25 mm thickness) were cut in squares of 10 mm  $\times$  10 mm to fit the sample holders and cleaned with an ultrasonic bath using isopropanol. For the plasma cleaning the selected gases were oxygen and argon at pressures about  $5 \times 10^{-3}$  mbar and xenon at lower pressures (about  $10^{-4}$  mbar, within the detection limit of the Baratron gauge used) with a source power of 100W. p-type (B) Si wafers, with 10-20 Ohm cm resistivity from Silicon Materials Inc., PA, USA, were used. XPS experiments were performed using a SPECS PHOIBOS150 hemispherical analyser with a monochromatic X-ray source (1486.6 eV) operated at 300W. The reported binding energies have been determined with an error of  $\pm 0.07$  eV, as derived from the used energy step (0.05 eV) and statistics, and are referred to the Fermi level ( $E_F$ ) of the analyser, which is periodically determined by measuring the photoelectron energies from an atomically clean reference Au(111) sample. No

---

<sup>1</sup> <http://ibssgroup.com/products/gv10x/>

charge correction has been applied for the binding energies. The estimated overall energy resolution (analyser and photons) is better than 0.6 eV at a pass energy of 20 eV.

The plasma source was installed on top of the fast-entry lock chamber of the ICN2 XPS system, as shown in Fig. 1. The distance from the DN40CF plasma source flange to the samples (centre of the viewport at the bottom left of the figure) was 62 cm in a direct line-of-sight geometry, in order to compare to parallel ex situ plasma cleaning experiments performed at ALBA-CELLS [12]. After plasma cleaning the samples were transferred first to a preparation chamber (bottom right of the figure), where they were stored in the low  $10^{-9}$  mbar range and transferred one by one to the analysis chamber, with a base pressure of  $2 \times 10^{-10}$  mbar during the XPS measurements. Scanning Electron Microscopy (SEM) micrographs and Energy Dispersive X-ray Spectroscopy (EDS) analysis of selected surfaces were obtained with a FEI Quanta 650FEG environmental SEM at ICN2.

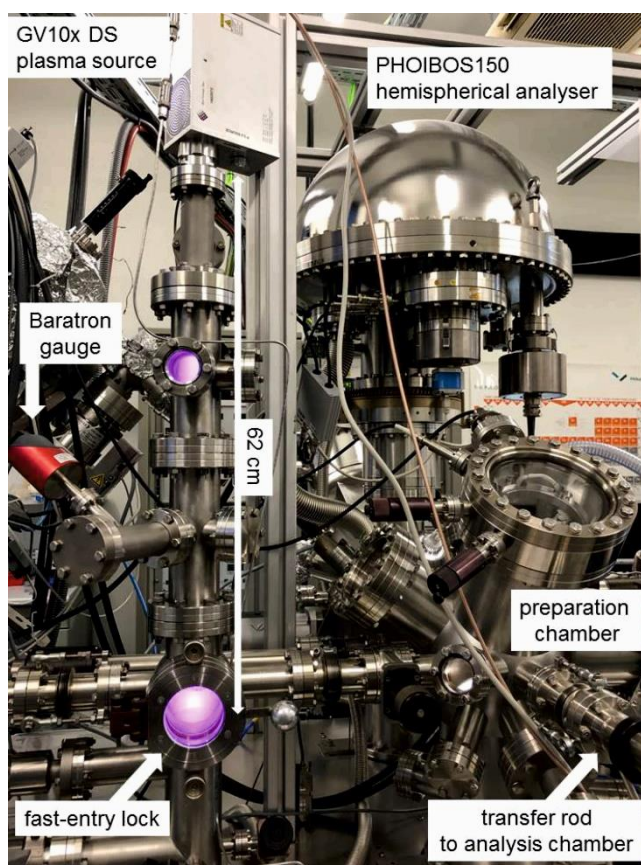
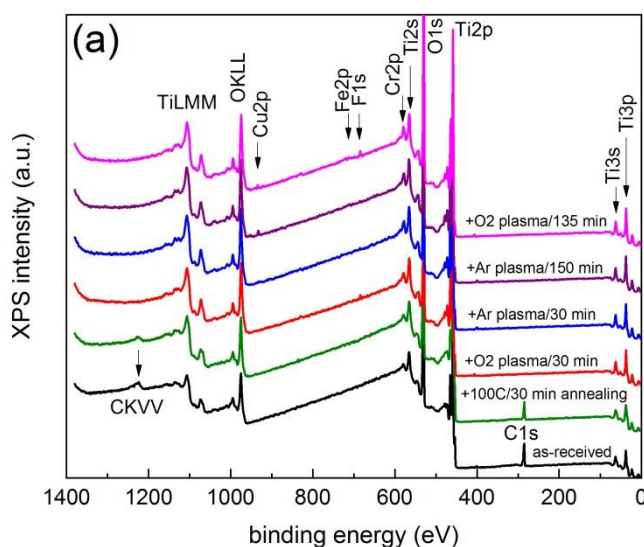


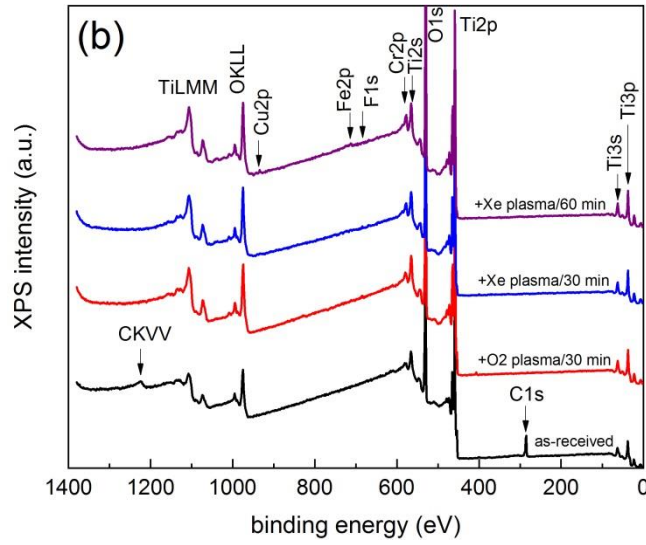
**Fig. 1.** Image of the ICN2 XPS system showing the GV10x DS Asher plasma source attached to the fast-entry lock system generating a xenon plasma (100W), whose light emission can be observed in the two viewports. The distance from the DN40CF flange of the source to the sample holder of the manipulator was set to 62 cm.

### 3. Results and discussion

#### 3.1 Ti-coated SS304L samples

Figure 2 shows the experimental XPS survey spectra of two different Ti-coated samples after a sequential exposure to (a) oxygen and argon plasma and (b) oxygen and xenon plasma, respectively. In Fig. 2(a) the spectrum corresponding to the as-received sample is represented by a black line while those spectra subsequently obtained after an in situ UHV annealing at 100 degrees C for 30 min, after exposure to oxygen plasma for 30 min, to argon plasma for 30 min, to additional 150 min of argon plasma and to further oxygen plasma treatment for 135 min are represented by olive, red, blue, purple and magenta lines, respectively. Following the same criterion, in Fig. 2(b) the spectra corresponding to the as-received sample, after exposure to oxygen plasma for 30 min, to xenon plasma for 30 min and to additional 60 min of xenon plasma are represented by black, red, blue and purple lines, respectively.

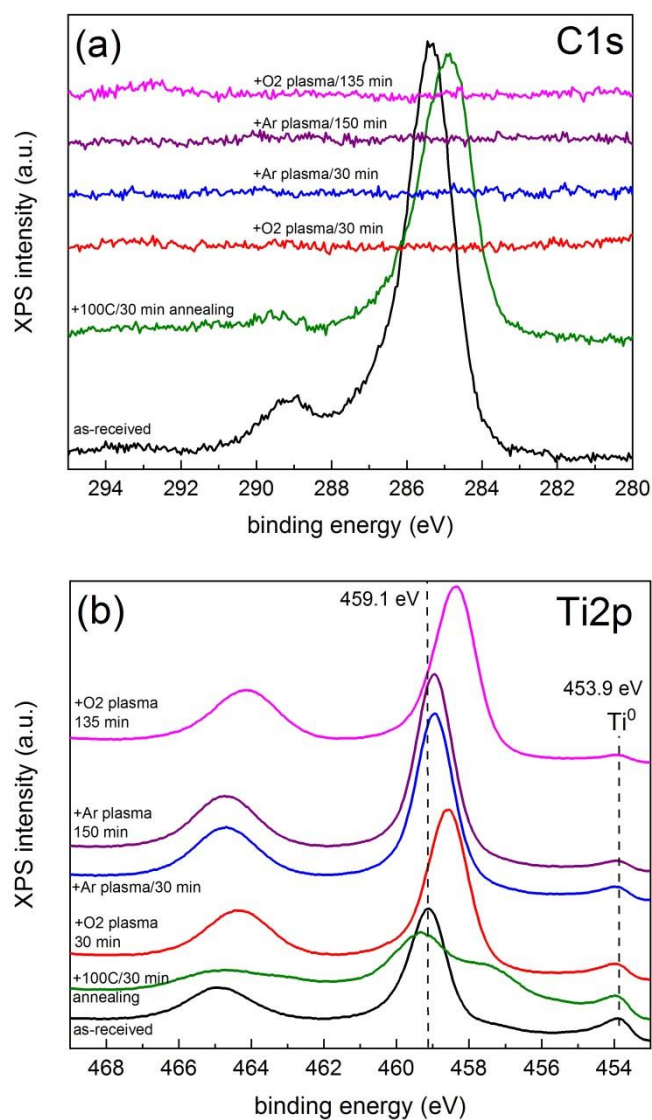




**Fig. 2.** Survey in situ XPS spectra of two different Ti thin films grown on stainless steel 304L foils after a sequential exposure to (a) oxygen and argon plasmas and (b) oxygen and xenon plasmas, respectively. The corresponding plasma treatment conditions are indicated for each spectrum. Spectra have been shifted in the vertical axis for clarity.

From Fig. 2(a) we notice that the C1s signal observed in the as-received spectrum decreases below the detection limit after the oxygen plasma treatment and that traces of fluorine (F1s) become detected at a binding energy around 690 eV. After 30 min argon plasma treatment, traces of copper are observed (Cu2p, about 933 eV binding energy), which become more apparent after the additional 150 min argon treatment. The presence of copper signal originates from the sputtering of the oxygen-free high conductivity (OFHC) gaskets in the fast-entry lock chamber by the plasma. From Fig. 2(b) we observe a similar general trend, but the effect of the sputtering of the surrounding inner walls becomes more evident with the presence of Cu2p, Fe2p and Cr2p lines [18]. Note that the second exposure to the xenon plasma is for a shorter period (60 min) as compared to the argon case (150 min). Thus, the xenon plasma induces a higher sputtering rate as compared to argon taking into account that the power of the source is kept constant at a fixed value of 100 W in both cases. This is essentially due to the different masses involved (xenon is more massive than argon) and to the resulting different plasma intensities (more intense light emission for xenon even at lower pressures).

Figures 3(a), (b) and (c) show the detailed evolution of the C1s, Ti2p and O1s lines, respectively, corresponding to the oxygen/argon sequential plasma treatment. The colour codes of the lines are the same as for Fig. 2(a). The analogous evolution corresponding to the oxygen/xenon plasma cleaning is represented in Fig. S1 (Supplementary Information).





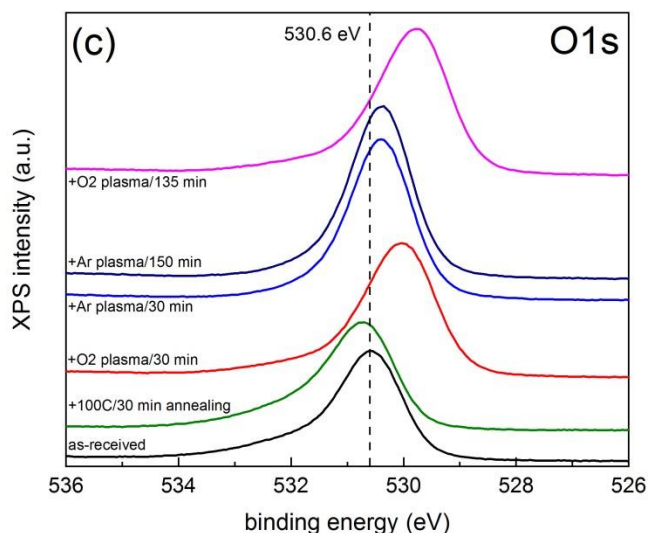


**Fig. 3.** High-resolution XPS spectra of the detailed in situ evolution of the (a) C1s, (b) Ti2p and (c) O1s lines, respectively. The corresponding plasma treatment conditions are indicated for each spectrum. The spectra have been shifted in the vertical axis by different offsets for clarity. Discontinuous vertical lines at 459.1, 453.9 and 530.6 eV are shown to help in tracking the shifts of the Ti2p and O1s spectra, respectively.

The C1s line corresponding to the as-received sample (black line) exhibits two main features at 285.4 and 289.1 eV in Fig. 3(a) which are assigned to C-C/C-H and O=C-O/CO<sub>3</sub><sup>2-</sup>, bonding, respectively [22]. After an in situ annealing at 100 degrees C for 30 min, the main peak shifts to lower binding energies (284.9 eV) and the 289.1 eV peak decreases in intensity. After exposure to the oxygen plasma for 30 min, the C1s signal becomes undetectable, evidencing the efficient removal of carbon contamination. Further exposure to argon plasma does not introduce any carbon contamination and after an additional oxygen plasma treatment for 135 min traces of potassium are observed (K2p line at about 293 eV). The same trend is also observed for xenon plasma [see Fig. S1(a) in Supplementary Information section]. Both potassium and fluorine traces appear only after exposure to the plasma, so that we believe that they are generated in the plasma source. An inspection of experiments performed in our XPS system before and after our plasma treatment study shows no traces of both elements, so that our XPS system should not be the origin of such contamination.

The evolution of the Ti2p core levels is shown in Fig. 3(b). The as-received spectrum shows the prominent contribution from formal Ti<sup>+4</sup> oxidation states, with a binding energy of 459.1 eV for the Ti2p<sub>3/2</sub> component, and the contribution from buried metallic

(Ti<sup>0</sup>) states, with a binding energy of 453.9 eV, that can be used as an absolute reference for the binding energy scale. Intermediate oxidation states around 457 eV binding energy are also observed. After the in situ annealing at 100 degrees C for 30 min, the Ti<sup>+4</sup> contribution decreases and shifts towards higher binding energy values (459.3 eV) and the signature of intermediate oxidation (Ti<sup>+3</sup>) states becomes more evident, due to the generation of surface defects, such as oxygen vacancies [23]. Thus, the surface becomes partially reduced even at such low temperatures, a fact that has been previously reported for Ti-based films used as non-evaporable getter (NEG) coatings [24–27]. The nearly full surface reduction (activation) induced by an in situ annealing up to 500 degrees C on the Ti thin films is shown in Fig. S2 in the Supplementary Information section.

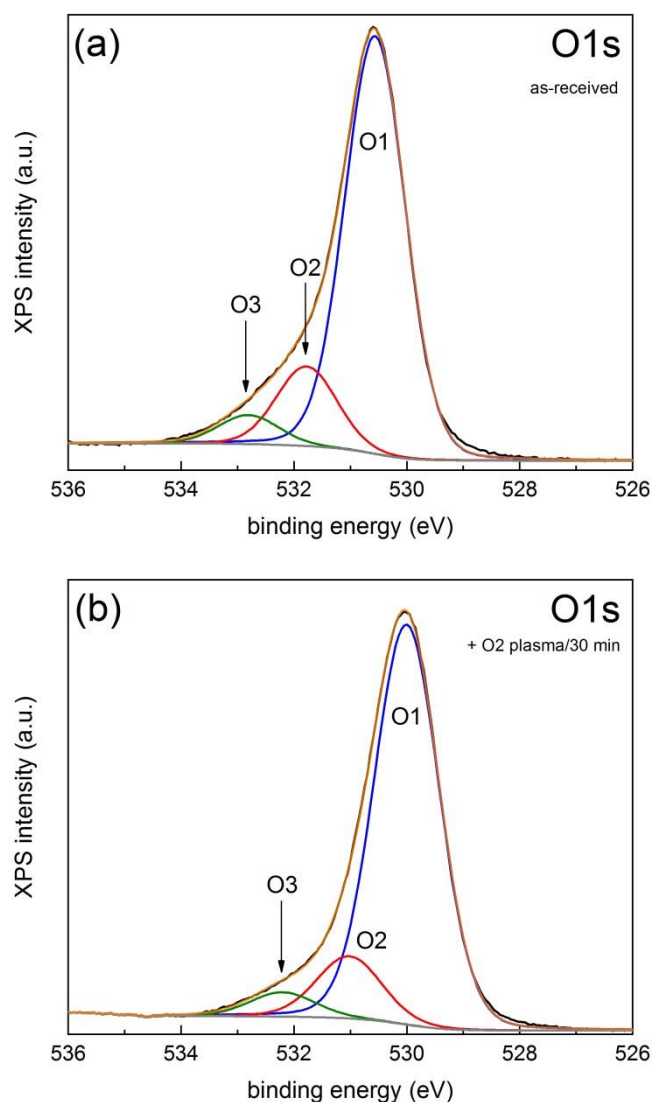
The 30 min oxygen plasma treatment reverts the situation by oxidizing back the surface with a shift of the Ti2p<sub>3/2</sub> main peak to lower binding energies (458.6 eV). The subsequent exposure to argon plasma induces a shift of the Ti2p components towards higher values, 459.0 eV, almost recovering the binding energy of the as-received surface and the final exposure to oxygen plasma for 135 min induces again a negative shift of the Ti2p lines down to a binding energy of 458.3 eV.

The exposure of the oxygen plasma treated surface to xenon plasma for 30 min also increases the binding energy from 458.6 eV to 458.8 eV (lower than for the analogous argon case) but decreases again the energy down to 458.5 eV after an additional 60 min exposure [see Fig. S1(b) in Supplementary Information section].

The O1s lines, as depicted from Fig. 3(c), show the similar trend as those observed in Fig. 3(b) for the Ti2p line. The initial binding energy corresponding to the main (metal-oxide) feature at 530.6 eV, shifts towards higher values (530.7 eV) after the annealing at 100 degrees C and decreases down to 530.0 eV after oxygen plasma treatment and shifts back to 530.4 eV after argon plasma. Finally, the main peak shifts back to lower binding energies (529.8 eV) after the 135 min oxygen plasma treatment. In the case of xenon plasma [see Fig. S1(c) in Supplementary Information section] the 530.0 eV value increases to 530.2 eV after 30 min of Xe plasma and decreases back to 530.0 eV after additional 60 min.

Figure 4 shows high-resolution XPS spectra of the O1s line (black line) of (a) the as-received sample, after sequential (b) oxygen and (c) argon plasma 30 min treatments,

respectively, with the corresponding least-squares fits using the *CasaXPS* software [28] after a Shirley-type background subtraction (grey line) using a combination of Gaussian (90%) and Lorentzian (10%) functions under the constraint of identical full width at half maximum (FWHM) for all components. The envelope from the fit is represented by the orange line, which closely follows the experimental data. Figures S3(a) and (b) in the Supplementary Information section display the binding energies and normalized areas of the components resulting from the fit, where additional results are included from the same batch, namely, the in situ annealing at 100 C before the exposure to the oxygen plasma for 30 min [Fig. 4(b)] as well as subsequent argon (150 min) and oxygen (135 min) plasma treatment after the 30 min argon plasma exposure from Fig. 4(c). The least-squares fits of the O1s lines corresponding to the combined oxygen/xenon plasma treatment is shown in Fig. S4 (Supplementary Information).



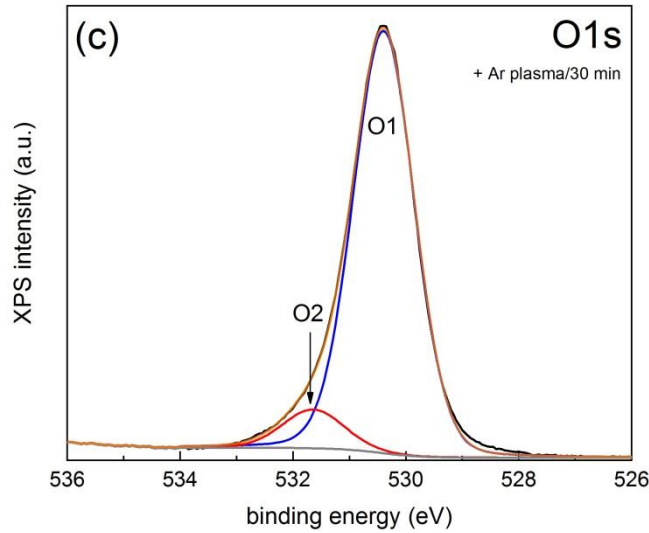


**Fig. 4.** High-resolution XPS spectra corresponding to the O1s core level of (a) the as-received sample and after sequential exposure for 30 min to (b) oxygen and (c) argon plasma, respectively. Details of the least-squares fits are given in the main text. The three components are represented by O1, O2 and O3, respectively.

### 3.2 Band bending in titanium films

The rigid negative shift of both the Ti2p and O1s core level binding energies by about 1 eV upon exposure to the oxygen plasma can be explained as due to band bending [29]. For a clean and stoichiometric TiO<sub>2</sub> surface the Ti2p<sub>3/2</sub> and the O1s peaks are located at 459.3 and 530.4 eV, respectively [30] and the generation of surface defects induces a rigid shift of the whole spectrum to lower binding energies: 458.5-458.7 eV for the Ti2p<sub>3/2</sub> line [23,25,31]. Here, the oxygen plasma, through its reactive species [10], generates defects at the surface and sub-surface (oxygen vacancies, trapped charges, etc.) moving the surface bands upward, as in a n-type semiconductor, thus increasing the measured kinetic energies of the photoelectrons resulting in lower binding energies. Both the argon and xenon plasmas are able to partially decrease the density of surface defects, inducing a healing of the surface with the consequent decrease of band bending.

In Fig. 4(a) features with 530.6 (O1, blue), 531.8 (O2, red) and 532.8 eV (O3, olive) binding energies are identified, with a common FWHM of 1.26 eV. The O1 component is assigned to lattice oxygen while O2 arises from contributions from oxygen vacancies, hydroxides and carbonates [22,31–34]. The higher binding energy feature O3 has been assigned either to adsorbed oxygen and/or water, to C-O bonding [32] and to

hydroxides [31]. However, we believe that it arises from oxygen associated to lower Ti oxidation states (+1 and +2), as will be discussed below. After the 30 min oxygen plasma treatment, the three components shift to lower binding energies: 530.0, 531.0 and 532.2 eV, respectively, due to the band bending caused by surface defects, with a common FWHM of 1.35 eV, as shown in Fig. 4(b). The increase of the FWHM is a signature of a more defective surface. After the subsequent argon plasma only two components are observed, O1 and O2, namely at 530.4 and 531.6 eV, respectively, with a FWHM of 1.27 eV.

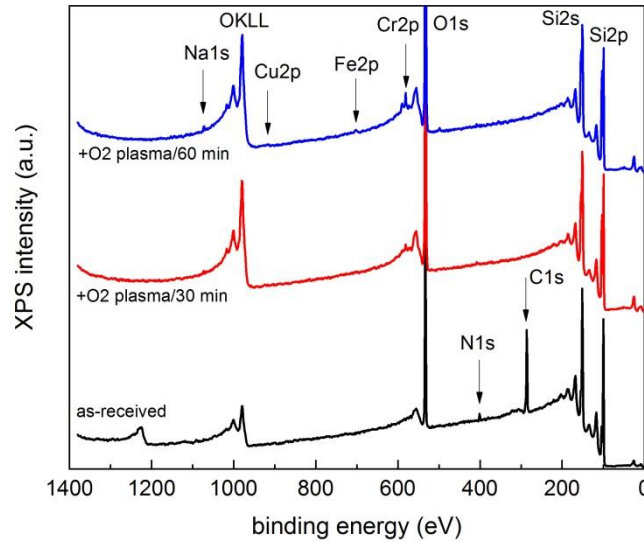
The evolution of the binding energies of the three components is summarized in Fig. S3(a), where O1, O2 and O3 are represented by full blue squares, red circles and olive triangles, respectively. Note that the energies shift to lower values upon exposure to the oxygen plasma and partially recover after the argon plasma treatment. O3 disappears after the argon plasma treatment, strongly suggesting the decrease of surface damage, as further confirmed by a decrease of the corresponding FWHM (1.27 eV). From Fig. S3(b) we observe that after the in situ annealing at 100 degrees C the area corresponding to O1 decreases by a small amount, but that the intensities of both O2 and O3 increase, which is a clear indication of the generation of reduced titanium states, as already depicted from Fig. 3(b). Upon exposure to oxygen plasma, the intensity of O1 increases while O2 and O3 decrease due to partial oxidation. Exposure to argon plasma increases O1 and decrease O2 eliminating O3, thus further oxidizing the surface. The subsequent exposure to oxygen plasma surprisingly decreases the O1 intensity and increases the contribution of both O2 and O3, which shows that the oxygen plasma generates oxygen vacancies with the consequent density of reduced states. This trend is also observed in Fig. 3(b), where the intensity of the  $Ti^{+4}$  feature increases with argon plasma treatment and exhibits lower values after exposure to oxygen plasma.

In summary, the experimental results indicate that oxygen plasma induces an upward band bending at the surface through the generation of surface defects whereas argon plasma helps to recover the  $TiO_2$  stoichiometry.

### 3.3 Si-coated SS304L samples

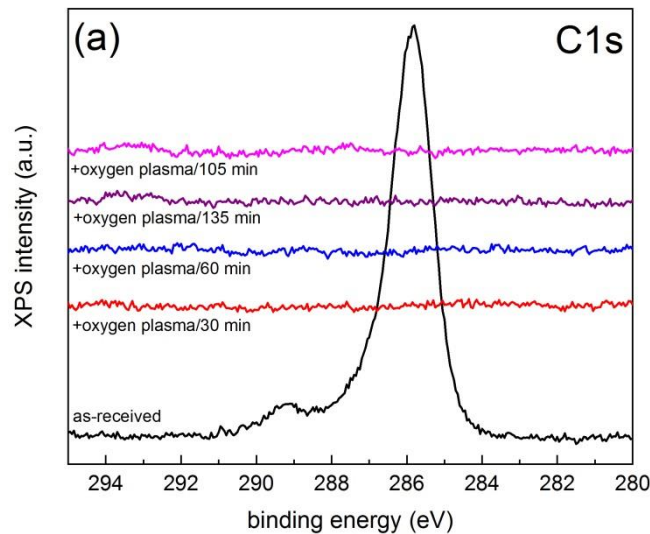
Figure 5 shows the evolution of the XPS survey spectra of a Si-coated SS304L sample after exposure to oxygen plasma. After 30 min plasma cleaning we observe the removal

of carbon and nitrogen but after additional 60 min Cr, Fe, Cu and Na are detected [18]. As mentioned in the previous section, the transition metal signals arise from sputtering of the surrounding walls and the origin of Na is unclear.



**Fig. 5.** Survey in situ XPS spectra of a Si-coated SS304L sample: as-received (black line), after 30 min oxygen plasma (red line) and after additional 60 min oxygen plasma (blue line). The spectra have been shifted in the vertical axis by an offset for clarity.

Figures 6(a), (b), (c) and (d) show the detailed evolution of the C1s, Si2p, O1s and N1s lines, respectively, corresponding to oxygen plasma treatment with sequential exposures of 30 (red line), 60 (blue line), 135 (purple) and 105 min (magenta line), respectively. Black lines represent the spectra of the as-received samples.



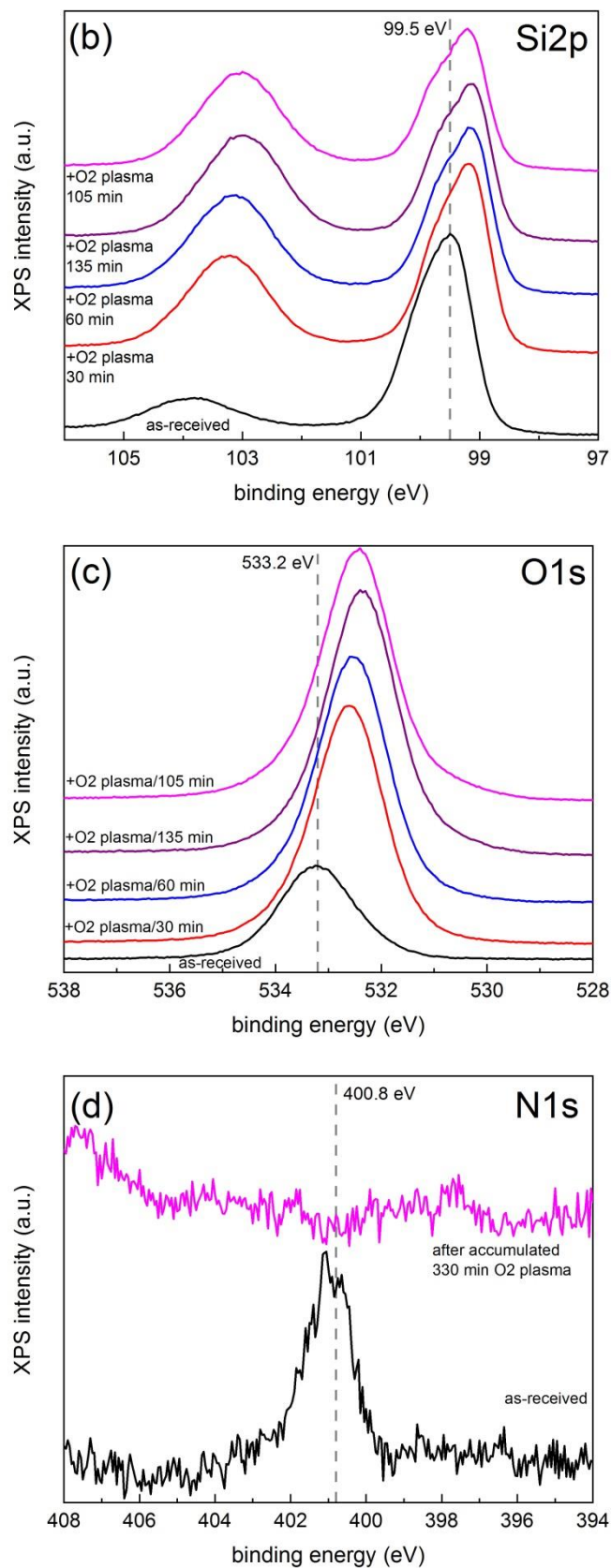


**Fig.6.** Evolution of the XPS C1s (a), Si 2p (b), O1s (c) and N1s (d) lines of a Si-coated SS304L sample after exposure to oxygen plasma for different periods. The corresponding plasma treatment conditions are indicated for each spectrum. The spectra have been shifted in the

vertical axis by an offset for clarity. Discontinuous grey vertical lines at 99.5, 533.2 and 400.8 eV are shown to guide the eye.

Figure 6(a) clearly shows that after exposure to the oxygen plasma for 30 min, carbon contamination is efficiently removed, and indeed, after further exposure to the same plasma the surface is kept carbon-free and with no subsequent segregation of C from deeper layer as a function of increasing plasma cleaning time. After an accumulated exposure of 330 min, traces of potassium are observed, as previously reported for the Ti-coated SS304L samples. From the Si2p line in Fig. 6(b) corresponding to the as-received sample we can estimate an oxide layer of about 1.1 nm [35]. The Si2p<sub>3/2</sub> component of the buried pure silicon exhibits a binding energy of 99.5 eV while the energy corresponding to the Si2p core level of the on-top silicon oxide is 103.8 eV. After 30 min exposure to the oxygen plasma, the signal corresponding to the oxide increases leading to an estimated thickness of about 2.9 nm and both lines shift towards lower binding energies: 99.2 and 103.2 eV, respectively. Further exposure to plasma leaves the positions essentially unchanged (99.1-99.2 eV and 103.0-103.2 eV). We thus observe a differential negative shift of 0.3-0.4 eV for sub-surface silicon and 0.6-0.8 eV for the oxide component. The O1s lines, as depicted from Fig. 6(c), show the similar trend as that observed in Fig. 6(b) for the Si2p line. The initial binding energy corresponding to the main feature at 533.2 eV decreases down to 532.6 eV after oxygen plasma treatment for 30 min and the additional plasma treatment maintains a shift between 0.6 and 0.9 eV. Finally, the N1s feature observed at 400.8 eV in the as-received sample [see Fig. 6(d)], which corresponds to molecularly chemisorbed nitrogen [36], is removed after oxygen plasma treatment.

Figure 7 shows high-resolution XPS spectra of the O1s line (black line) of (a) the as-received sample, (b) after 30 min oxygen plasma and (c) after an accumulated 330 min plasma treatment, respectively, with the corresponding least-squares fits after a Shirley-type background subtraction (grey line) using a combination of Gaussian (90%) and Lorentzian (10%) functions under the constraint of identical FWHM for all components. The envelope from the fit is represented by the orange line, which closely follows the experimental data.



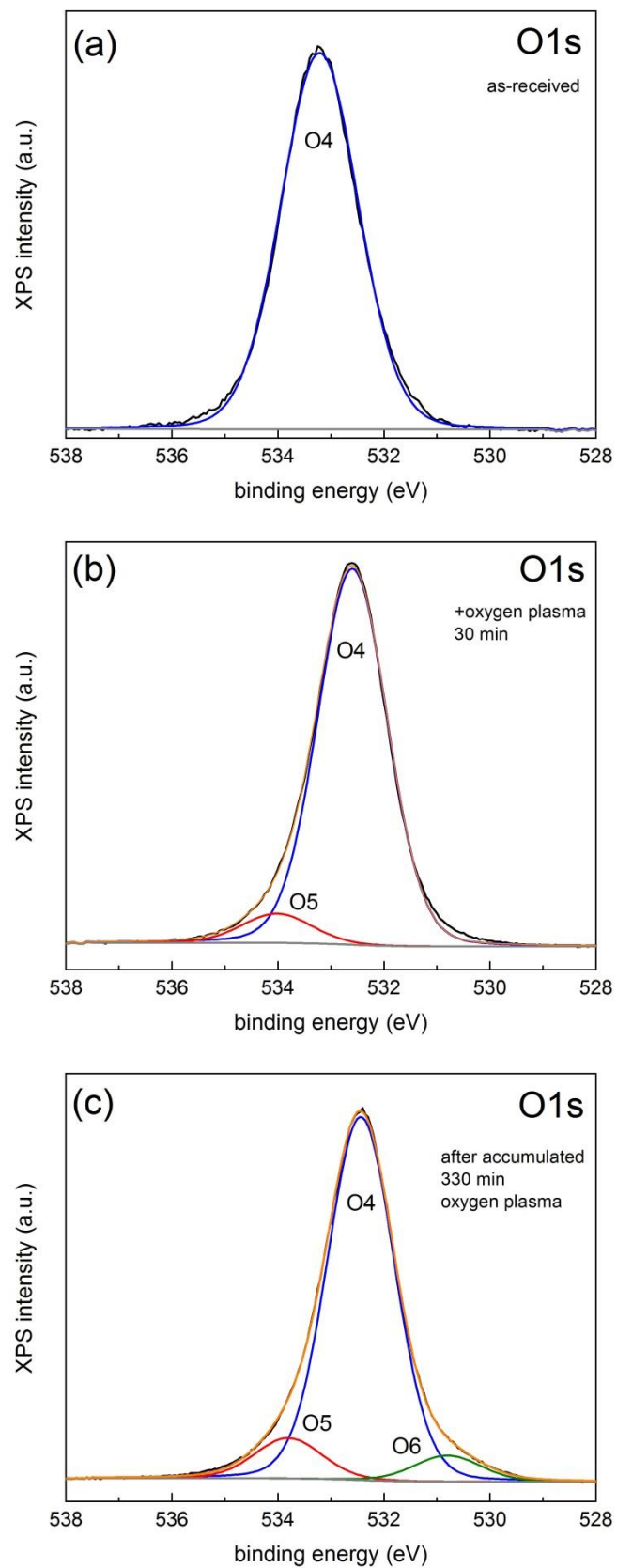


**Fig.7.** High-resolution XPS spectra corresponding to the O1s line (black line) of (a) the as-received sample, (b) after 30 min oxygen plasma and (c) after an accumulated 330 min plasma

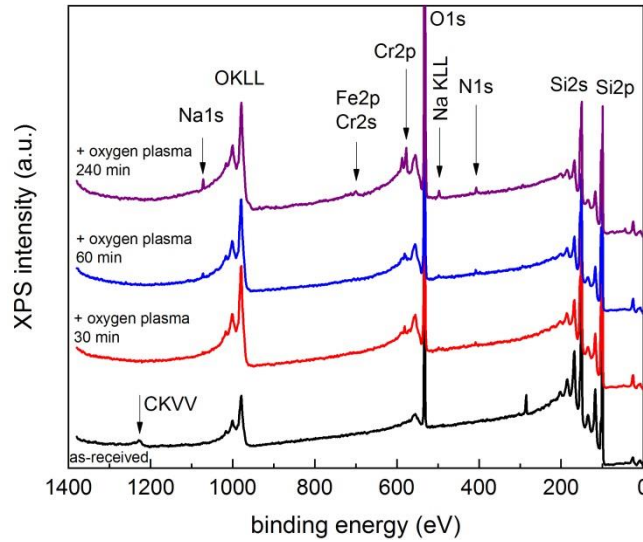
treatment, respectively. Details of the least-squares fits are given in the main text. The three components are represented by O4, O5 and O6, respectively.

In Fig. 7(a) the fit can be satisfactorily performed using a single component, with a binding energy of 533.2 eV (O4) and a FWHM of 1.72 eV, which corresponds to the well-accepted energy of silicon oxide. After the 30 min oxygen plasma treatment, the main component shifts down to 532.6 eV and an extra component appears at 534.0 eV (O5) with a common FWHM of 1.54 eV [Fig. 7(b)]. The origin of the 534.0 eV feature will be discussed later. After an accumulated oxygen plasma dose of 330 min an extra component appears at 530.8 eV (O6), as shown in Fig. 7(c), apart from the previous lines located at 532.4 (main) and 533.8 eV, respectively, with a common FWHM of 1.49 eV. The 530.8 eV can be assigned to metal oxides (mainly  $\text{CrO}_x$ ) due to sputtering, as can be inferred from Fig. 5.

In addition to the Si-coatings on SS304L foils referred above, Silcolloy® 1000 coatings have been also deposited on stainless steel DN16CF and DN40CF flanges and on a DN63CF 6-way cross. Details on the morphology and composition of the coatings as well as on the determined outgassing rates can be found in the Supplementary Information Section (see Fig. S5).

### *3.4 p-type Si wafers*

Before analysing the data shown in the previous section, it is illustrative to discuss analogous experiments performed with p-type Si wafers with the same experimental conditions, i.e., both Si-coatings and wafers were exposed to the oxygen plasma at the same time and measured in the same run. Figure 8 shows the evolution of the XPS survey spectra after sequential exposure to oxygen plasma. After 30 min plasma cleaning we observe the removal of carbon and the progressive presence of Cr, Fe, Cu and Na contamination.

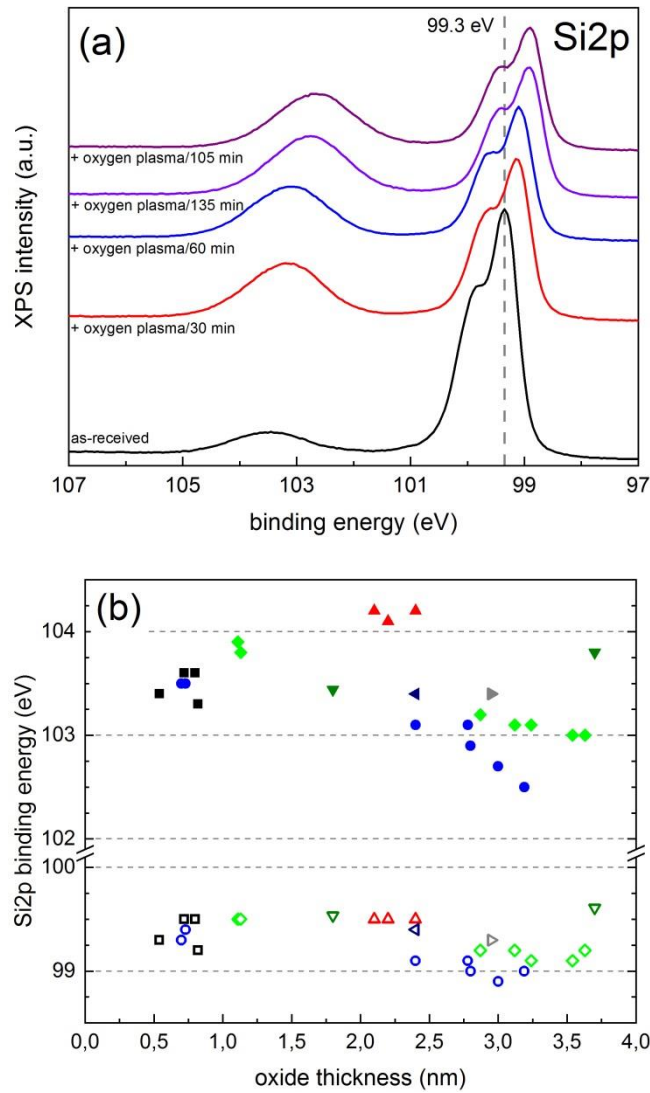


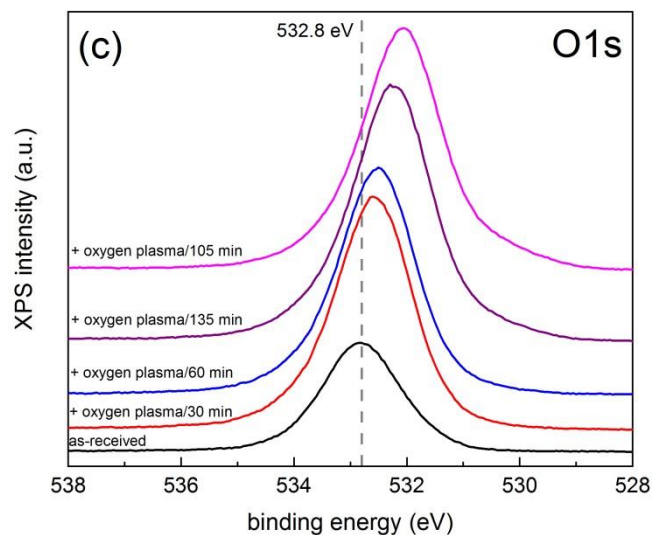
**Fig.8.** Survey in situ XPS spectra of a p-type Si wafer sample: as-received (black line) and after 30 min (red line), additional 60 min (blue line) and 240 min (purple line) oxygen plasma. The spectra have been shifted in the vertical axis by an offset for clarity.

Figure 9(a) below shows the evolution of the Si2p lines in terms of the sequentially acquired spectra after cumulative exposure to oxygen plasma. From the figure we can observe a clear tendency of a shift towards lower binding energies as the dose increases, with an initial value of 99.3 eV for the Si2p core level of pristine silicon corresponding to the as-received sample. This value reproduces previous results, obtained in a different photoemission system, performed on wafers from the same batch that were half-covered with a thin platinum film whose Pt4f<sub>7/2</sub> line (71.0 eV) was used as an internal energy reference [37]. The lines shift by -0.4 and -0.8 eV corresponding to pure silicon and silicon oxide, respectively. This tendency is compared to selected data from the literature in Fig. 9(b), where the binding energies are represented as a function of the oxide thickness. Full and open symbols represent the Si2p binding energies corresponding to Si and SiO<sub>2</sub>, respectively. Data from Fig. 9(a) together with additional data acquired with other silicon wafers from the same batch (i.e., same doping) are represented by blue circles. Black squares correspond to as-received Si wafers measured in the same XPS system in the last 5 years and red up-triangles, olive down-triangles and navy left-triangles to data from refs. [37], [38] and [39], respectively. The figure includes the data from Fig. 6(a), represented by green diamonds, and also the results from a silicon wafer treated ex situ in a different system but with the same distance from the plasma source DN40CF flange to the sample [12], with an Ar(10%)/O<sub>2</sub>(90%) gas

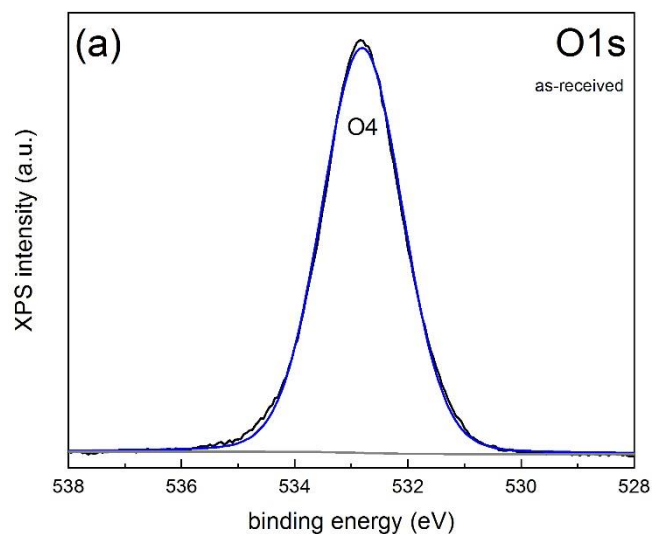
mixture (grey right-triangles). Finally, the evolution of the O1s line is shown in Fig. 9(c). In this case the observed shift is -0.7 eV.

Least-squares fits of the O1s line for the as-received (a) and after an accumulated exposure to the oxygen plasma for 330 min (b) are given in Figs. 10. The dependence of the binding energy of the main component (O4) as a function of the oxide thickness is represented in Fig. 11, where the data points are represented by crossed symbols following the same assignment as in Fig. 9(b).





**Fig.9.** Evolution of the XPS Si 2p line of a p-type Si wafer (a) after exposure to oxygen plasma for different amounts of time and (b) as a function of the estimated oxide thickness. (c) Evolution of the XPS O1s line after exposure to oxygen plasma. The spectra have been shifted in the vertical axis by an offset for clarity. Discontinuous vertical lines at 99.3 (a) and 532.8 eV (c) are shown to help in tracking the shifts of the Si2p and O1s spectra, respectively.



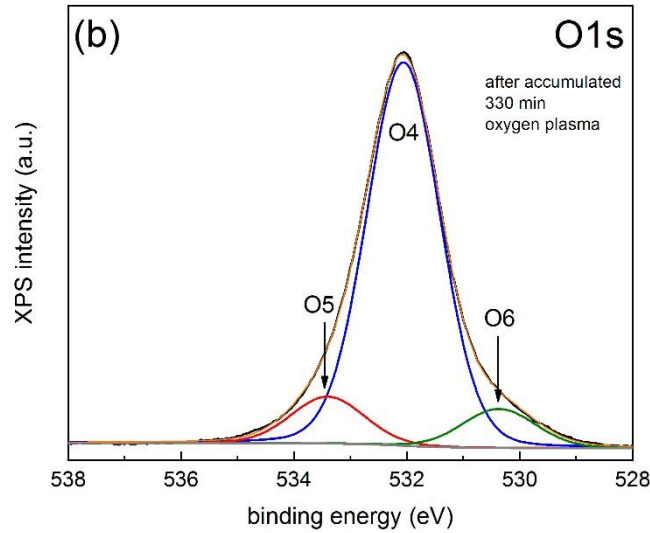


**Fig. 10.** High-resolution XPS spectra corresponding to the O1s line (black line) of (a) the as-received sample and (b) after an accumulated 330 min plasma treatment, respectively. Least-squares fits of the experimental data after a Shirley-type background subtraction (grey line) are shown using a combination of Gaussians (90%) and Lorentzian (10%) functions under the constraint of identical FWHM for all components. The envelop of the fit is represented by an orange line and the three components by blue (O4), red (O5) and olive (O6) lines, respectively. The emergence of the O5 feature is associated to the oxygen plasma, so that it can be interpreted as a defect state.

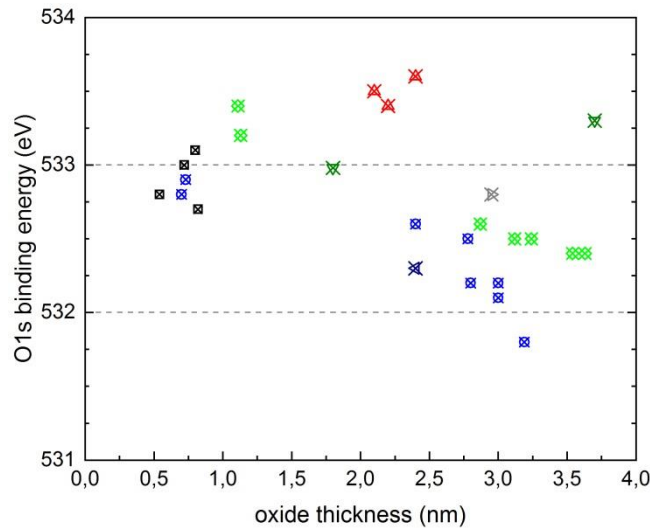


**Fig. 11.** Evolution of the main component of the XPS O1s line of a p-type Si wafer as a function of the estimated oxide thickness.

### *3.5 Band bending in Si wafers and coatings*

A gradually increasing value of the thickness of the oxide layer should lead to charging in the photoemission spectra, due to the insulating character of silicon oxide [40]. Due to the large difference in the band gap, 1.1 vs. 8.9 eV for Si and SiO<sub>2</sub>, respectively, the corresponding lines charge differently. This is exemplified with the results from refs. [38] (olive symbols) and [37] (red symbols), where the oxide layers have been grown *ex situ* by thermal annealing in dry oxygen and by *ex situ* oxygen plasma treatment for 1 min at 360 W, respectively. In the case of oxides grown by thermal annealing, the shifts corresponding to pure silicon and silicon oxide are 0.07 and 0.3 eV, respectively, between the 1.8 and 3.7 nm thickness range, while for a thickness of 40 nm, the binding energies are 104.0 and 533.5 eV for the Si2p and O1s lines, respectively, thus with a shift of 0.53 eV between 1.8 nm and 40 nm for both core levels [38]. In addition, one should expect a downward band bending for a p-type Si sample due to the fact that the oxide side of the SiO<sub>2</sub>/Si interface is positively charged due to electron injection from the oxide to the silicon part [41]. Thus, this downward band bending adds to the positive energy shift.

However, after the *in situ* oxygen plasma treatment for both the Si wafer and coatings discussed in the present work, the binding energies decrease, so that such behaviour should be rooted in a different phenomenon. It is well known that the surface photovoltage in p-type Si samples shifts the energy of the peaks to lower binding energies, i.e., towards a flat-band scenario [42]. In our case the samples were illuminated during the XPS measurements with the white light from the ion gauges in the analysis chamber as well as with light from the laboratory, so that this should induce a constant shift during all measurements. The surface photovoltage effect has been previously determined for wafers from the same batch by acquiring data with and without external light (ion gauges off and viewports from the analysis chamber masked). In this case the negative shift was less than 0.08 and 0.16 eV for the Si2p lines of the pristine and oxidized silicon, respectively (see Fig. S6).

It has been reported that the generation of defects and charges can induce shifts of both signs in the photoemission lines in Si/SiO<sub>2</sub> systems. Hirose claimed that the binding energies of the Si 2p core levels for Si substrates covered with ca. 1 nm SiO<sub>2</sub> either increase or decreases as the X-ray irradiation time from the XPS source increases and attributes such a change to the trapping of carriers generated by photoelectron emission

in the oxide film: a shift toward higher/lower binding energies indicates that the number of positive/negative charges in the oxide film is increasing [43]. Silicon and silicon oxide surfaces exposed to oxygen reactive ion etching plasma and stored under different humidity conditions show positive shifts of the oxide-related components as referred to the Si2p line of pristine silicon [44]. Argon plasma treated silicon substrates show positive shifts of about 0.4 eV using an inductively coupled reactor [45] while samples exposed to a gaseous mixture of nitrogen and oxygen at 300 degrees C using a plasma-enhanced chemical vapour deposition (PECVD) system show negative shifts [46]. Several works in the literature calibrate the binding energies to the Si2p core level energy of pristine silicon, sometimes to correct for charging, so that a direct comparison with our results is not possible [47].

We propose that the decrease of the measured binding energy of the core levels is due to the generation of defects caused by the impinging plasma species that induce vacancies and negative trapped charges that translates into an upward band bending. The estimated position of the valence band maximum (VBM) referred to  $E_F$  of pristine silicon buried under the native oxide for the p-type wafers used in this work is about 0.6 eV, as shown in Fig. S7. This value is obtained from the extrapolation of the edge of the XPS signal close to  $E_F$ . According to Himpsel et al. [48], the position of the Si2p<sub>3/2</sub> core level for highly-doped p-type Si(111) surfaces is 98.8 eV (referred to  $E_F$ ), so that our 99.3 eV value would locate the VBM 0.5 eV below  $E_F$ , in good agreement with our 0.6 eV estimate. An upward band bending would be limited by such a quantity since the bands cannot cross  $E_F$ , which is the case since for both the silicon wafers and films, the maximum negative shift is of 0.4 eV. The shifts corresponding to the oxidized part are not limited by the 0.5-0.6 eV value, since the band gap is much larger. Figure S10 includes the determination of the Si/SiO<sub>2</sub> valence band offset (4.6 eV) using monochromatic 21.22 eV photons, which is comparable to the value obtained from oxidized Si(100) surfaces, 4.3 eV [35].

In summary, oxygen plasma induces an upward band bending at the surface of both p-type silicon wafers and coatings as a result of the generation of surface defects.

#### 4. Conclusions



We have characterised the surface modification induced by a downstream inductively-coupled plasma on two selected materials, namely silicon and titanium, of interest as internal coatings of UHV chambers by in situ XPS. The goal is to determine such a modification avoiding the exposure to air. Titanium and silicon exhibit good adherence to stainless steel and reduce the outgassing rates. The study has been extended to silicon wafers in order to emulate surfaces of synchrotron and free-electron laser beamline optics and as a reference.

From our results, we can evidence the effective removal of carbon contamination using an oxygen plasma due to the absence of photoemission signal from C1s core levels. With the used 100 W power of the plasma source, we can establish an upper limit of 30 min to avoid the contamination caused by sputtering of the surrounding walls of the vacuum vessel for the particular experimental set-up, with a distance from source to sample of about 62 cm in a line-of-sight geometry. This contamination can be further reduced by using aluminium and/or alumina shields in the plasma source. Oxygen plasma induces defects at the surface of the oxide layers, generating vacancies and trapped charges, which are evidenced by an upward band bending (i.e., lower binding energies of the core levels). It is yet to be determined if such surface damage in silicon mirrors translates in a serious hindrance in their optical response and if the density of generated defects can be decreased by an additional plasma treatment (e.g., argon), as has been shown for titanium films.

## **Acknowledgements**

This research was supported by the Government of Catalonia's Industrial Doctorates Plan and by the Spanish Ministry of Economy and Competitiveness (MINECO) under Contract No. PGC2018-095032-B-100. The ICN2 is funded by the CERCA program/Generalitat de Catalunya. The ICN2 is supported by the Severo Ochoa program of MINECO (Grant SEV-2017-0706). We acknowledge A. Gevorgyan from ALBA-CELLS Vacuum Group for the outgassing measurements of the DN63CF 6-way cross.

## **References**

- [1] K. Boller, R.P. Haelbich, H. Hogrefe, W. Jark, C. Kunz, Investigation of carbon contamination of mirror surfaces exposed to synchrotron radiation, *Nucl. Instruments Methods Phys. Res.* 208 (1983) 273–279.  
[https://doi.org/10.1016/0167-5087\(83\)91134-1](https://doi.org/10.1016/0167-5087(83)91134-1).
- [2] C. Chauvet, F. Polack, M.G. Silly, B. Lagarde, M. Thomasset, S. Kubsky, J.P. Duval, P. Risterucci, B. Pilette, I. Yao, N. Bergéard, F. Sirotti, Carbon contamination of soft X-ray beamlines: Dramatic anti-reflection coating effects observed in the 1 keV photon energy region, *J. Synchrotron Radiat.* 18 (2011) 761–764. <https://doi.org/10.1107/S0909049511023119>.
- [3] W.K. Warburton, P. Pianetta, In situ optical element cleaning with photon activated oxygen, *Nucl. Inst. Methods Phys. Res. A.* 319 (1992) 240–243.  
[https://doi.org/10.1016/0168-9002\(92\)90560-Q](https://doi.org/10.1016/0168-9002(92)90560-Q).
- [4] A. Toyoshima, T. Kikuchi, H. Tanaka, J.I. Adachi, K. Mase, K. Amemiya, In situ removal of carbon contamination from optics in a vacuum ultraviolet and soft X-ray undulator beamline using oxygen activated by zeroth-order synchrotron radiation, *J. Synchrotron Radiat.* 19 (2012) 722–727.  
<https://doi.org/10.1107/S0909049512024971>.
- [5] E.D. Johnson, R.F. Garrett, In situ reactive cleaning of X-ray optics by glow discharge, *Nucl. Inst. Methods Phys. Res. A.* A266 (1988) 381–385.  
[https://doi.org/10.1016/0168-9002\(88\)90414-7](https://doi.org/10.1016/0168-9002(88)90414-7).
- [6] R.W.C. Hansen, J. Umhoefer, Maintaining a carbon free beamline with in situ cleaning, in: *AIP Conf. Proc.*, 2000: p. 128. <https://doi.org/10.1063/1.1291772>.
- [7] T. Koide, T. Shidara, M. Yanagihara, S. Sato, Resuscitation of carbon-contaminated mirrors and gratings by oxygen-discharge cleaning 2: Efficiency recovery in the 100–1000-eV range, *Appl. Opt.* 27 (1988) 4305–4313.  
<https://doi.org/10.1364/ao.27.004305>.
- [8] B. Anthony, In situ cleaning of silicon substrate surfaces by remote plasma-excited hydrogen, *J. Vac. Sci. Technol. B Microelectron. Nanom. Struct.* 7 (1989) 621–626. <https://doi.org/10.1116/1.584805>.
- [9] F. Eggenstein, F. Senf, T. Zeschke, W. Gudat, Cleaning of contaminated XUV-optics at BESSY II, *Nucl. Instruments Methods Phys. Res. Sect. A Accel.*

- Spectrometers, Detect. Assoc. Equip. 467–468 (2001) 325–328.  
[https://doi.org/10.1016/S0168-9002\(01\)00312-6](https://doi.org/10.1016/S0168-9002(01)00312-6).
- [10] E. Pellegrin, I. Šics, J. Reyes-Herrera, C. Pérez Sempere, J.J. López Alcolea, M. Langlois, J. Fernández Rodríguez, V. Carlino, Characterization, optimization and surface physics aspects of in situ plasma mirror cleaning, *J. Synchrotron Radiat.* 21 (2014) 300–314. <https://doi.org/10.1107/S1600577513032402>.
  - [11] M.G. Cuxart, J. Reyes-Herrera, I. Šics, A.R. Goñi, H.M. Fernandez, V. Carlino, E. Pellegrin, Remote plasma cleaning of optical surfaces: Cleaning rates of different carbon allotropes as a function of RF powers and distances, *Appl. Surf. Sci.* 362 (2016) 448–458. <https://doi.org/10.1016/j.apsusc.2015.11.117>.
  - [12] H. Moreno Fernández, M. Zangrando, G. Sauthier, A.R. Goñi, V. Carlino, E. Pellegrin, Towards chemically neutral carbon cleaning processes: plasma cleaning of Ni, Rh and Al reflective optical coatings and thin Al filters for free-electron lasers and synchrotron beamline applications, *J. Synchrotron Radiat.* 25 (2018) 1642–1649. <https://doi.org/10.1107/S1600577518014017>.
  - [13] H. Ohashi, Y. Senba, H. Yumoto, T. Koyama, T. Miura, H. Kishimoto, Development of contamination-free x-ray optics for next-generation light sources, in: *AIP Conf. Proc.*, 2016: p. 040023. <https://doi.org/10.1063/1.4952895>.
  - [14] H. Li, A. Belkind, F. Jansen, Z. Orban, An in situ XPS study of oxygen plasma cleaning of aluminum surfaces, *Surf. Coatings Technol.* 92 (1997) 171–177. [https://doi.org/10.1016/S0257-8972\(97\)00079-0](https://doi.org/10.1016/S0257-8972(97)00079-0).
  - [15] S. Wolf, M. Edmonds, X. Jiang, R. Droopad, N. Yoshida, L. Dong, R. Galatage, S. Siddiqui, B. Sahu, A. Kummel, (Invited) Rapid In-Situ Carbon and Oxygen Cleaning of In<sub>0.53</sub>Ga<sub>0.47</sub>As(001) and Si<sub>0.5</sub>Ge<sub>0.5</sub>(110) Surfaces via a H<sub>2</sub> RF Downstream Plasma, *ECS Trans.* 72 (2016) 291–302. <https://doi.org/10.1149/07204.0291ecst>.
  - [16] R. James, F.L. Pasquale, J.A. Kelber, Plasma-enhanced chemical vapor deposition of ortho-carborane: Structural insights and interaction with Cu overlayers, *J. Phys. Condens. Matter.* 25 (2013) 355004. <https://doi.org/10.1088/0953-8984/25/35/355004>.
  - [17] B. Dong, M.S. Driver, I. Emesh, R. Shaviv, J.A. Kelber, Surface chemistry and

- fundamental limitations on the plasma cleaning of metals, *Appl. Surf. Sci.* 384 (2016) 294–297. <https://doi.org/10.1016/j.apsusc.2016.05.082>.
- [18] K.B. Becker, Synchrotron radiation mirrors for high intensity beam lines, *Rev. Sci. Instrum.* 63 (1992). <https://doi.org/10.1063/1.1143032>.
- [19] H. Ohashi, Y. Senba, Y. Kotani, T. Miura, H. Kishimoto, T. Koyama, Effective protocol for realizing contamination-free X-ray reflective optics, *Rev. Sci. Instrum.* 90 (2019) 021704. <https://doi.org/10.1063/1.5063262>.
- [20] S.K. Sharma, B.C. Chakravarty, S.N. Singh, B.K. Das, Oxidation of silicon in RF induced oxygen plasma, *J. Mater. Sci. Lett.* 9 (1990) 982–984. <https://doi.org/10.1007/BF00722196>.
- [21] D.W. Hess, Plasma-assisted oxidation, anodization, and nitridation of silicon, *IBM J. Res. Dev.* 43 (1999) 127–145. <https://doi.org/10.1147/rd.431.0127>.
- [22] M. Macías-Montero, C. López-Santos, A.N. Filippin, V.J. Rico, J.P. Espinós, J. Fraxedas, V. Pérez-Dieste, C. Escudero, A.R. González-Elipe, A. Borrás, In Situ Determination of the Water Condensation Mechanisms on Superhydrophobic and Superhydrophilic Titanium Dioxide Nanotubes, *Langmuir*. 33 (2017) 6449–6456. <https://doi.org/10.1021/acs.langmuir.7b00156>.
- [23] J.T. Mayer, U. Diebold, T.E. Madey, E. Garfunkel, Titanium and reduced titania overlayers on titanium dioxide(110), *J. Electron Spectros. Relat. Phenomena*. 73 (1995) 1–11. [https://doi.org/10.1016/0368-2048\(94\)02258-5](https://doi.org/10.1016/0368-2048(94)02258-5).
- [24] C. Benvenuti, J.M. Cazeneuve, P. Chiggiato, F. Cicoira, A.E. Santana, V. Johanek, V. Ruzinov, J. Fraxedas, Novel route to extreme vacua: the non-evaporable getter thin film coatings, *Vacuum*. 53 (1999) 219–225. [https://doi.org/10.1016/S0042-207X\(98\)00377-7](https://doi.org/10.1016/S0042-207X(98)00377-7).
- [25] M.P. Lozano, J. Fraxedas, XPS analysis of the activation process in non-evaporable getter thin films, *Surf. Interface Anal.* 30 (2000) 623–627. [https://doi.org/10.1002/1096-9918\(200008\)30:1<623::AID-SIA719>3.0.CO;2-Y](https://doi.org/10.1002/1096-9918(200008)30:1<623::AID-SIA719>3.0.CO;2-Y).
- [26] J. Wang, Y. Gao, Z. You, J. Fan, J. Zhang, Z. Qiao, S. Wang, Z. Xu, Non-evaporable getter Ti-V-Hf-Zr film coating on laser-treated aluminum alloy

- substrate for electron cloud mitigation, *Coatings*. 9 (2019) 839.  
<https://doi.org/10.3390/coatings9120839>.
- [27] J.Q. Shao, X.Q. Ge, W. Wei, B. Zhang, S.H. Wang, Y.X. Zhang, B.L. Zhu, C. Chen, W.M. Li, Y. Wang, Preparation of Titanium-Zirconium-Vanadium films by quantitative deposition, in: *J. Phys. Conf. Ser.*, 2019: p. 012166.  
<https://doi.org/10.1088/1742-6596/1350/1/012166>.
- [28] J. Walton, P. Wincott, N. Fairley, A. Carrick, *Peak Fitting with CasaXPS*, Accolyte Science, Knutsford, UK, 2010.
- [29] Z. Zhang, J.T. Yates, Band bending in semiconductors: Chemical and physical consequences at surfaces and interfaces, *Chem. Rev.* 112 (2012) 5520–5551.  
<https://doi.org/10.1021/cr3000626>.
- [30] U. Diebold, The surface science of titanium dioxide, *Surf. Sci. Rep.* 48 (2003) 53–229. [https://doi.org/10.1016/s0167-5729\(02\)00100-0](https://doi.org/10.1016/s0167-5729(02)00100-0).
- [31] M. Ishfaq, M. Rizwan Khan, M.F. Bhopal, F. Nasim, A. Ali, A.S. Bhatti, I. Ahmed, S. Bhardwaj, C. Cepek, 1.5MeV proton irradiation effects on electrical and structural properties of TiO<sub>2</sub>/n-Si interface, *J. Appl. Phys.* 115 (2014) 174506. <https://doi.org/10.1063/1.4874942>.
- [32] M. Chen, X. Wang, Y.H. Yu, Z.L. Pei, X.D. Bai, C. Sun, R.F. Huang, L.S. Wen, X-ray photoelectron spectroscopy and auger electron spectroscopy studies of Al-doped ZnO films, *Appl. Surf. Sci.* 158 (2000) 134–140.  
[https://doi.org/10.1016/S0169-4332\(99\)00601-7](https://doi.org/10.1016/S0169-4332(99)00601-7).
- [33] G. Ketteler, S. Yamamoto, H. Bluhm, K. Andersson, D.E. Starr, D.F. Ogletree, H. Ogasawara, A. Nilsson, M. Salmeron, The nature of water nucleation sites on TiO<sub>2</sub>(110) surfaces revealed by ambient pressure X-ray photoelectron spectroscopy, *J. Phys. Chem. C*. 111 (2007) 8278–8282.  
<https://doi.org/10.1021/jp068606i>.
- [34] J.C. Dupin, D. Gonbeau, P. Vinatier, A. Levasseur, Systematic XPS studies of metal oxides, hydroxides and peroxides, *Phys. Chem. Chem. Phys.* 2 (2000) 1319–1324. <https://doi.org/10.1039/a908800h>.
- [35] F.J. Himpsel, F.R. McFeely, A. Taleb-Ibrahimi, J.A. Yarmoff, G. Hollinger,

- Microscopic structure of the SiO<sub>2</sub>/Si interface, *Phys. Rev. B.* 38 (1988) 6084–6096. <https://doi.org/10.1103/PhysRevB.38.6084>.
- [36] E. Martínez-Ferrero, Y. Sakatani, C. Boissière, D. Grosso, A. Fuertes, J. Fraxedas, C. Sanchez, Nanostructured titanium oxynitride porous thin films as efficient visible-active photocatalysts, *Adv. Funct. Mater.* 17 (2007) 3348–3354. <https://doi.org/10.1002/adfm.200700396>.
- [37] J. Fraxedas, K. Zhang, B. Sepúlveda, M.J. Esplandiu, X.G. De Andrés, J. Llorca, V. Pérez-Dieste, C. Escudero, Water-mediated photo-induced reduction of platinum films, *J. Synchrotron Radiat.* 26 (2019) 1288–1293. <https://doi.org/10.1107/S1600577519004685>.
- [38] J.L. Alay, M. Fukuda, C.H. Bjorkman, K. Nakagawa, S. Yokoyama, S. Sasaki, M. Hirose, Determination of valence band alignment at ultrathin SiO<sub>2</sub>/Si interfaces by high-resolution x-ray photoelectron spectroscopy, *Jpn. J. Appl. Phys.* 34 (1995) L653–L656. <https://doi.org/10.1143/JJAP.34.L653>.
- [39] A. Verdaguer, C. Weis, G. Oncins, G. Ketteler, H. Bluhm, M. Salmero, Growth and structure of water on SiO<sub>2</sub> films on Si investigated by kelvin probe microscopy and in situ X-ray spectroscopies, *Langmuir.* 23 (2007) 9699–9703. <https://doi.org/10.1021/la700893w>.
- [40] T.L. Barr, An XPS study of Si as it occurs in adsorbents, catalysts, and thin films, *Appl. Surf. Sci.* 15 (1983) 1–35. [https://doi.org/10.1016/0378-5963\(83\)90003-X](https://doi.org/10.1016/0378-5963(83)90003-X).
- [41] H. Sezen, S. Suzer, Communication: Enhancement of dopant dependent x-ray photoelectron spectroscopy peak shifts of Si by surface photovoltage, *J. Chem. Phys.* 135 (2011) 141102. <https://doi.org/10.1063/1.3652964>.
- [42] M. Çopuroğlu, H. Sezen, R.L. Opila, S. Suzer, Band-bending at buried SiO<sub>2</sub>/Si interface as probed by XPS, *ACS Appl. Mater. Interfaces.* 5 (2013) 5875–5881. <https://doi.org/10.1021/am401696e>.
- [43] K. Hirose, XPS time-dependent measurement of SiO<sub>2</sub>/Si and HfAlO<sub>x</sub>/Si interfaces, *J. Electron Spectros. Relat. Phenomena.* 176 (2010) 46–51. <https://doi.org/10.1016/j.elspec.2009.06.003>.
- [44] A.U. Alam, M.M.R. Howlader, M.J. Deen, Oxygen Plasma and Humidity

Dependent Surface Analysis of Silicon, Silicon Dioxide and Glass for Direct Wafer Bonding, ECS J. Solid State Sci. Technol. 2 (2013) P515–P523.

<https://doi.org/10.1149/2.007312jss>.

- [45] K.J. Trevino, J.C. Shearer, B.D. Tompkins, E.R. Fisher, Comparing isoelectric point and surface composition of plasma modified native and deposited SiO<sub>2</sub> films using contact angle titrations and X-ray photoelectron spectroscopy, Plasma Process. Polym. 8 (2011) 951–964. <https://doi.org/10.1002/ppap.201100010>.
- [46] B. Stegemann, K.M. Gad, P. Balamou, D. Sixtensson, D. Vössing, M. Kasemann, H. Angermann, Ultra-thin silicon oxide layers on crystalline silicon wafers: Comparison of advanced oxidation techniques with respect to chemically abrupt SiO<sub>2</sub>/Si interfaces with low defect densities, Appl. Surf. Sci. 395 (2017) 78–85. <https://doi.org/10.1016/j.apsusc.2016.06.090>.
- [47] S.A. Nelson, H.D. Hallen, R.A. Buhrman, A structural and electrical comparison of thin SiO<sub>2</sub> films grown on silicon by plasma anodization and rapid thermal processing to furnace oxidation, J. Appl. Phys. 63 (1988) 5027. <https://doi.org/10.1063/1.340450>.
- [48] F.J. Himpsel, G. Hollinger, R.A. Pollak, Determination of the Fermi-level pinning position at Si(111) surfaces, Phys. Rev. B. 28 (1983) 7014–7018. <https://doi.org/10.1103/PhysRevB.28.7014>.